Astron. Astrophys. 296, 33–44 (1995)

ASTRONOMY
AND
ASTROPHYSICS

The molecular front in galaxies

I. CO vs HI in position-velocity diagrams

Yoshiaki Sofue, Mareki Honma, and Nobuo Arimoto

Institute of Astronomy, University of Tokyo, Mitaka, Tokyo 181, Japan
e-mail: sofue@mtk.ioa.s.u-tokyo.ac.jp

Received 18 July 1994 / Accepted 9 September 1994

Abstract. We have obtained composite position-velocity (PV) diagrams of the HI and CO line emissions for edge-on galaxies NGC 891, NGC 4565, NGC 5907, and NGC 3079. Using a de-convolving method of the PV diagram, we have obtained radial distributions of HI and H_2 gas densities, and the radial variation of the molecular fraction as defined by the mass ratio of the molecular (H_2) to total (HI + H_2) gas density has been calculated. Radial variations of the molecular fraction shows that the galaxy disk is almost totally molecular in the central few kpc region. However, the molecular fraction decreases suddenly in a narrow range of radius, beyond which the interstellar gas is almost totally HI, and we call this critical radius the 'molecular front'. We point out that the molecular and atomic gases in disk galaxies are clearly separated by this front, which will be the place where the phase transition from HI to H_2, and vice versa, is taking place in the galactic scale. We discuss the implication of the molecular-front phenomenon for the evolution of interstellar gas in galaxies based on the phase-transition theory of the ISM.

Key words: galaxies: ISM – galaxies: spiral – ISM: molecules – radio lines: galaxies

1. Introduction

The atomic hydrogen (HI) gas has been mapped in the 21-cm line emission for a large number of galaxies with the use of interferometers at high angular resolutions. It is also long since a number of galaxies have been mapped in the molecular lines at mm-wavelengths, particularly in the ^{12}CO($J = 1 - 0$) line emission. The CO line data, such as those obtained at high angular resolutions with the Nobeyama 45-m and IRAM 30-m telescopes, have been used to obtain distributions of the molecular hydrogen gas on the assumption that the CO intensity is proportional to the molecular hydrogen column mass.

It has been well known that the HI gas is distributed in the outer region of galaxies, while it is deficient in the central several kpc (e.g., Bosma 1981). On the other hand, the molecular gas is known to be more concentrated in the central several kpc region, often showing a nuclear concentration in the central 1 kpc making a nuclear disk and/or a compact ring (Young & Scoville 1992; Sofue 1991). Although this general tendency has been known, there has been no quantitative analyses of the distribution of molecular fraction and of the phase transition from HI to H_2 and from H_2 to HI gases.

In this paper, we report on the result of a detailed comparison of the HI and CO (molecular gas) distributions in several edge-on galaxies in composite (CO plus HI) position-velocity (PV) diagrams. The CO emission generally originates in high-density interstellar regions, while the HI in more diffuse interstellar gas, and therefore, a CO-plus-HI PV diagram represents the "true" distribution of interstellar gas. Using the observed PV diagrams, we derive the radial distribution of gas densities of H_2 and HI, and further, the molecular gas fraction. We point out that the HI to H_2 transition, and vice versa, is taking place in a narrow range of radius in the galactic disk, which we call the 'molecular front'. On this basis we discuss the physics of the phase transition of the interstellar gas in a galactic scale.

2. CO vs HI in the position-velocity diagrams

For the study of radial variations of various quantities such as the density and molecular fraction, we have made use of position-velocity diagrams obtained for edge-on galaxies of Sb and Sc types. In Figs. 1 to 7 we present composite PV diagrams, in which CO and HI PV diagrams are superposed for NGC 891, NGC 4565, NGC 5907, NGC 3079, as well as for M 31 and the Milky Way Galaxy. We stress that this kind of systematic and simultaneous plots of both the HI and CO emissions in PV diagrams in the same scale have been obtained in the present paper for the first time.

Primarily, these diagrams are useful to obtain rotation properties of the galaxies both in HI and CO: Figs. 1 to 7 indicate that the CO as well as HI rotation curves already attain the maximum at the galacto-centric distance $R \sim 3 - 10$ kpc, and are

Send offprint requests to: Y. Sofue

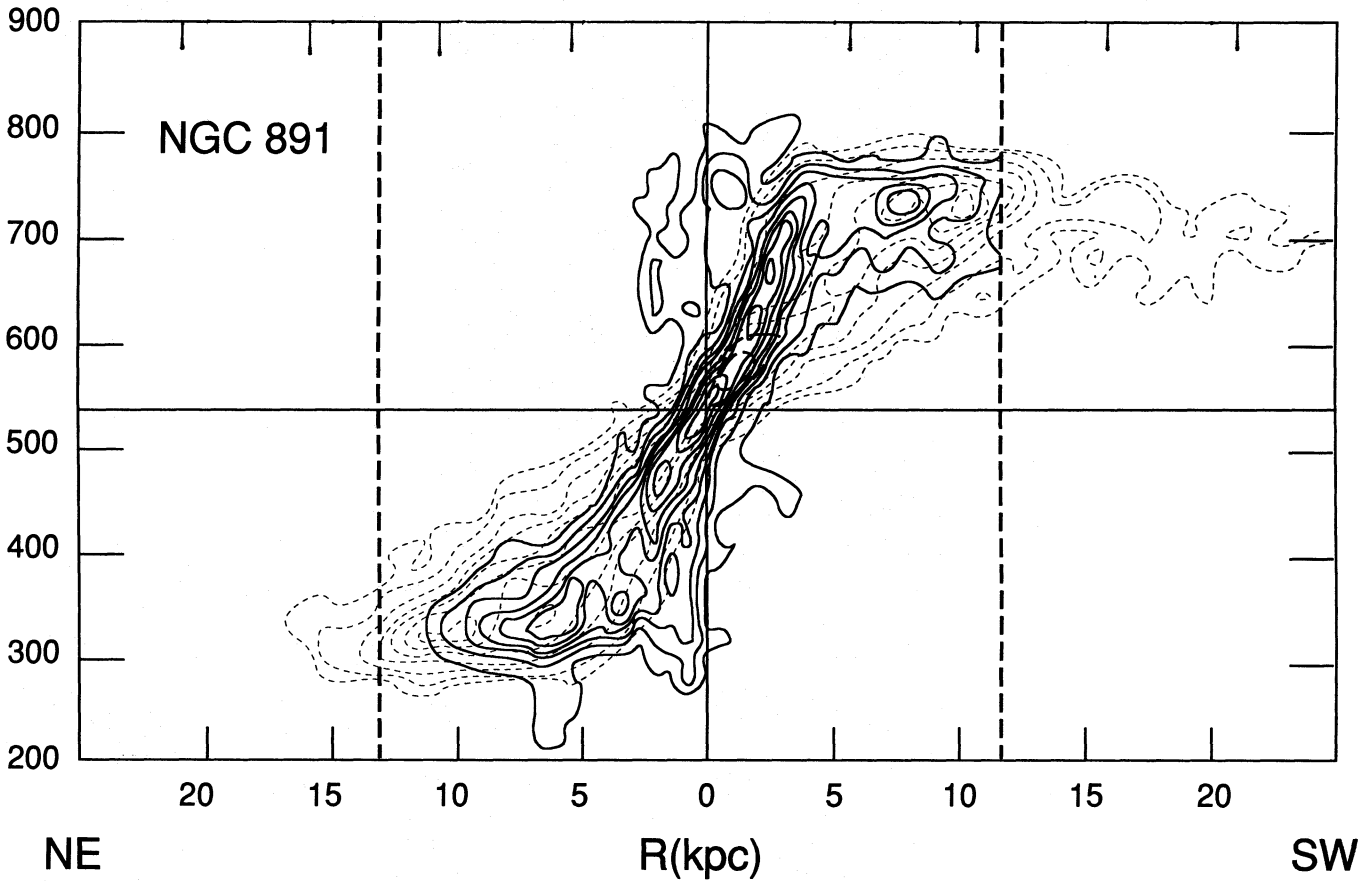

Fig. 1. CO + HI PV diagram for NGC 891. Dashed contours are for HI, thick contours ours for CO. Vertical lines indicate the region of CO observations. Abscissa indicates the distance along the major axis with bottom tick marks every 5 kpc and top tick marks every 2 min arc. The ordinate indicates LSR velocity in km s^{-1}. The same applies to Figs. 2 to 4

followed by a flat rotation of the outer gas. The fact that both the HI and CO emitting regions attain the same maximum rotation velocity at $R \sim 5 - 10$ kpc have been used to argue for a coincidence of the total line profiles in CO and HI and has been used to establish the CO-line Tully Fisher relation (Sofue 1992; Schöniger & Sofue 1993). The diagrams can also be used for deriving dynamical as well as structural informations such as about a bar potential and a bar-shocked gas ring in the central region. In this paper we use these diagrams for deriving the molecular and HI gas fractions in the galaxy disks as functions of the distance from the galactic center.

2.1. NGC 891

This is a typical Sb galaxy with an almost perfect edge-on orientation, and is supposed to be the most similar galaxy to the Milky Way. This galaxy has been extensively mapped in the CO line (Garcia-Burillo et al. 1991; Sofue & Nakai 1992; Scoville et al. 1993) and in the HI line (Sancisi 1976; Rupen 1991). Figure 1 shows a composite PV diagram of the CO and HI lines. The CO PV diagram has been taken from the Nobeyama 45-m telescope data at a 15″ resolution obtained by Sofue & Nakai (1993), and the HI diagram from the VLA data at a 20″ resolution obtained by Rupen (1991). The CO diagram is characterized by the 4-kpc molecular ring feature, which makes an apparently rigid-rotation ridge running across the origin of the diagram. In addition to this ring, the central high-velocity enhancement is evident, which comprises a steep and rigid rotation feature at $R < 1$ kpc corresponding to the rapidly-rotating nuclear disk. The HI gas is distributed in a larger radius region in a broad ring and outskirts at $R > 10$ kpc. The rotation curve of the galaxy is almost flat at $R < 15$ kpc, and is followed by a gradually declining rotation in the outermost region.

It is remarkable that the 4-kpc CO ring is located just inside the main HI ring, and that the HI and CO gases generally avoid each other. It is also impressive that the CO nuclear ring is not associated with HI at all: the HI emission is not detected in the central 3 kpc, indicating depression of HI gas in the center.

2.2. NGC 4565

This is an Sb galaxy at a distance of 10.2 Mpc and with a large inclination angle of $i \simeq 86°$. Figure 2 shows the CO+HI composite PV diagram. The CO data have been taken from the Nobeyama 45-observations by Sofue & Nakai (1993) and HI from the VLA observations by Rupen (1991). The CO PV dia-

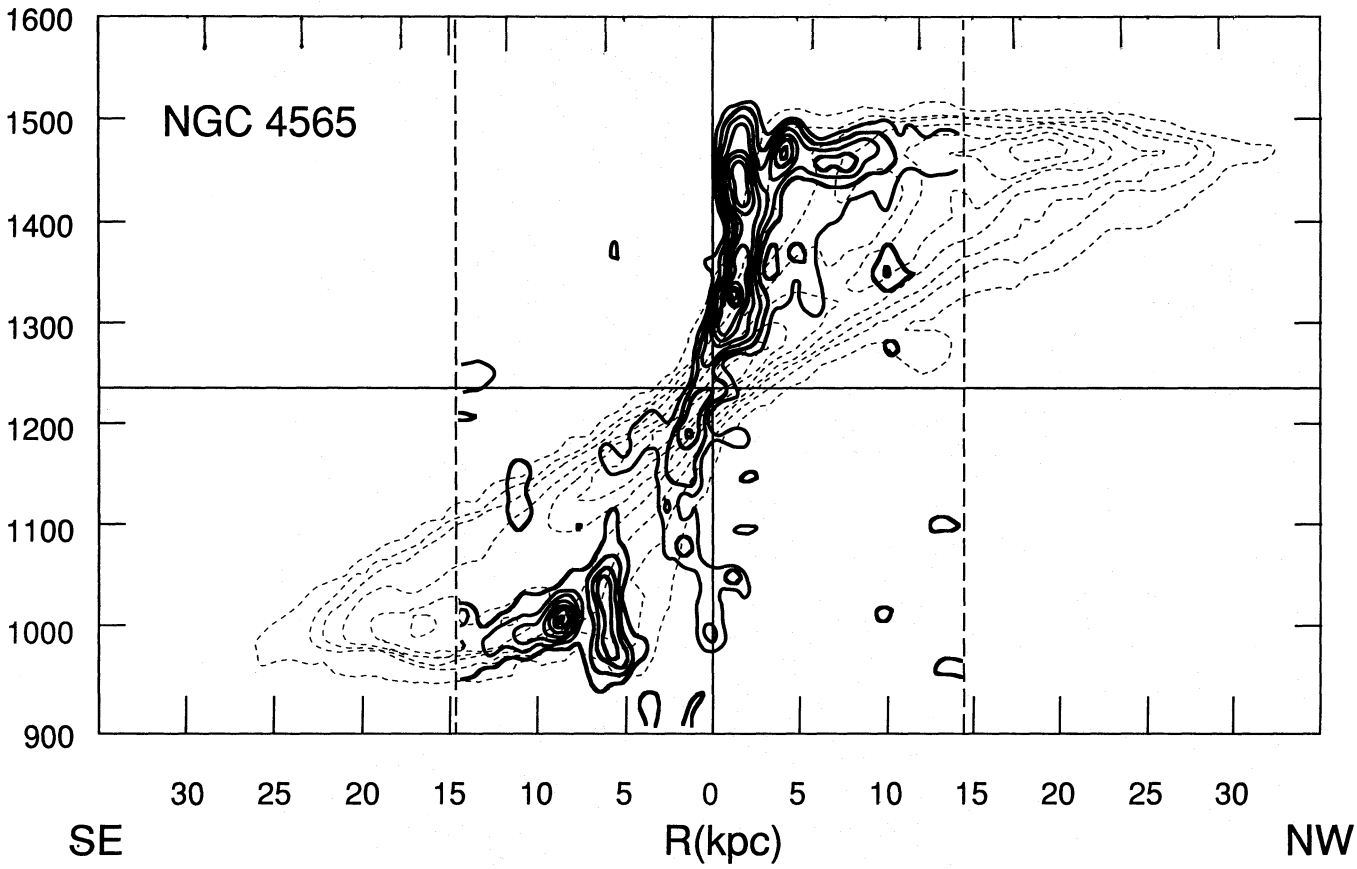

Fig. 2. CO + HI PV diagram for NGC 4565

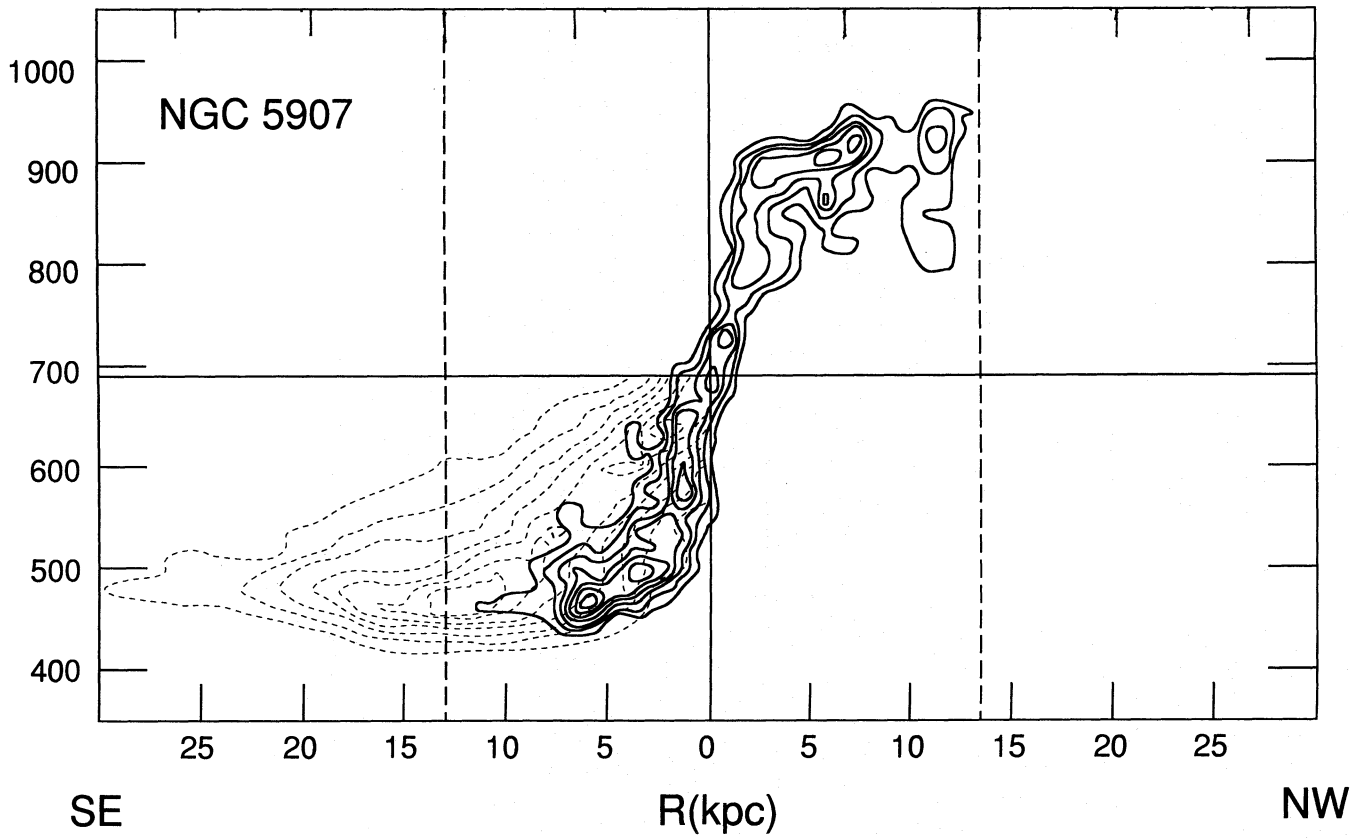

Fig. 3a. CO + HI PV diagram for NGC 5907

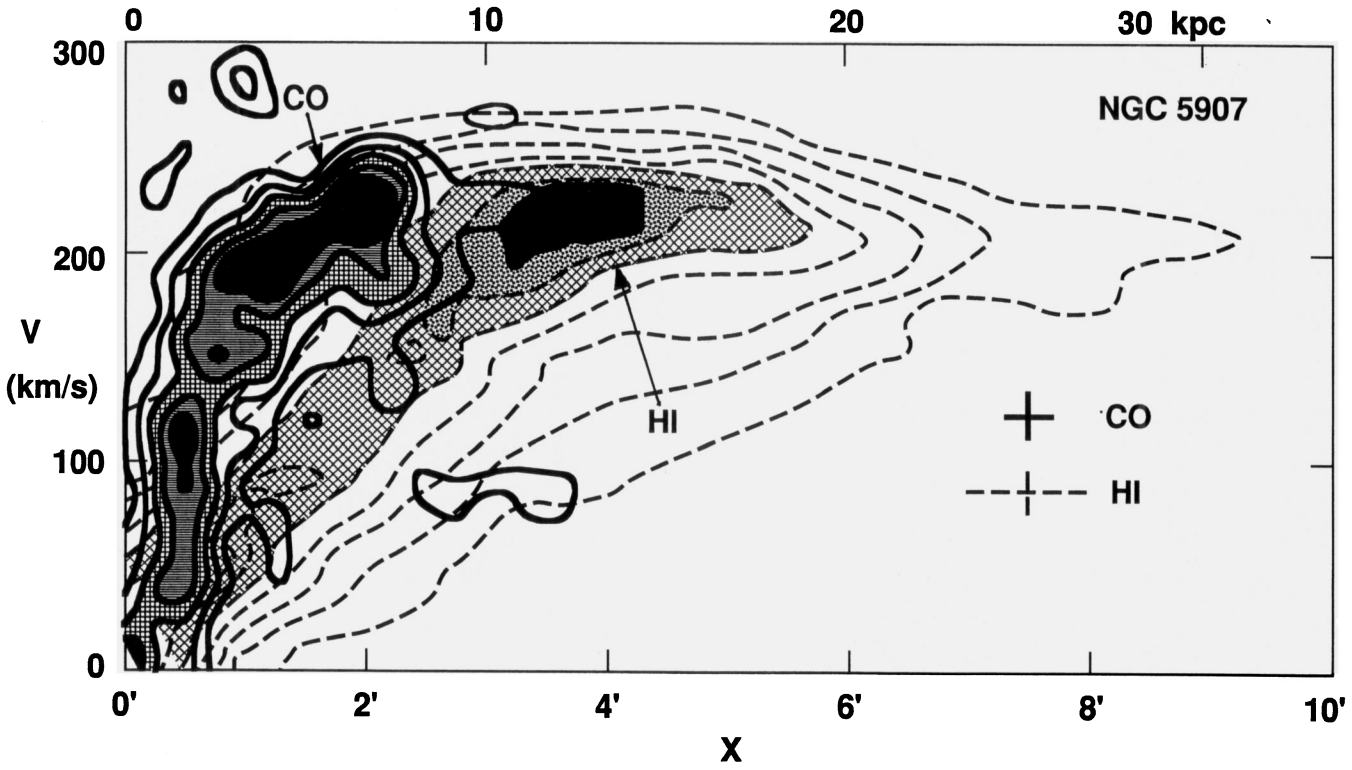

Fig. 3b. CO + HI PV diagram for NGC 5907 for the north-western part

gram shows a significant lopsidedness in the sense that the CO in the SW side is lacking. However, the HI diagram shows an almost perfect symmetry. Again, the displacement between the CO and HI is evident. Particularly, the nuclear CO disk is not associated with HI gas.

2.3. NGC 5907

Figure 3a shows the CO+HI composite PV diagram for NGC 5907, and Fig. 3b its enlargement for the south-eastern part. The CO data have been taken from the Nobeyama 45-m observations by Sofue (1994a), and the HI data from the WSRT observations as presented in Casertano (1983). (No HI data are available in the literature for the north-western side.) This diagram demonstrates the overall displacement of molecular and atomic hydrogen gases most clearly. The HI gas is distributed over a large ring of 12 kpc radius, while the CO gas makes up a ring of 4 to 7 kpc radius. It is peculiar that this galaxy shows a central depression also in the CO line.

2.4. M 31

The HI line emission from M 31 has been extensively mapped with single dish telescopes (Roberts 1978) as well as with interferometers (Brinks & Bajaja 1986). Sofue & Kato (1981) derived a face-on distribution of the HI gas, showing that the HI gas is strongly concentrated in the 10 to 12-kpc ring. The CO emission has been mapped by Dame et al. (1993), and position-velocity diagrams as cut along and parallel to the major axis have been presented. Figure 4 shows the composite PV diagram of the HI and CO emissions along the major axis, as reproduced from Dame et al. (1993).

The PV diagram shows an HI ring at $R = 12$ kpc, and a CO ring at $R \sim 10$ kpc radius, indicating that the molecular gas is located at the inner (smaller-radius) edge of the HI ring. However there is little HI and CO emission in the inner 10 kpc of M 31. In the central few minutes (Sofue & Yoshida 1993; Sofue et al. 1994b; Sofue 1994b) M 31 shows evidence for accretion of gas clouds from companions which may have disrupted the usual inner gas disk. Further away from the nucleus, Allen & Lequeux (1993) have detected weak CO emission from dust clouds and found that the amount of molecular gas can be substantial, the weakness of the CO emission being due to the lack of heating sources.

2.5. NGC 3079

This is an amorphous edge-on galaxy classified as Sc type. It has an active galactic nucleus associated with two symmetrical radio lobes emerging perpendicularly to the galactic plane (Duric et al. 1983). The nuclear region is also associated with a molecular gas outflow (Irwin & Sofue 1992). Figure 5a and b show composite CO+HI PV diagrams for NGC 3079, where the HI diagram has been taken from Irwin & Seaquist (1991) at a resolution of 20″ from the VLA. The CO diagram in Fig. 5a has been taken from the data observed with the Nobeyama mm Array at an angular resolution of 4″ for the central 1′ region (Sofue & Irwin 1992). In these data the CO emission is not detected in the outer regions

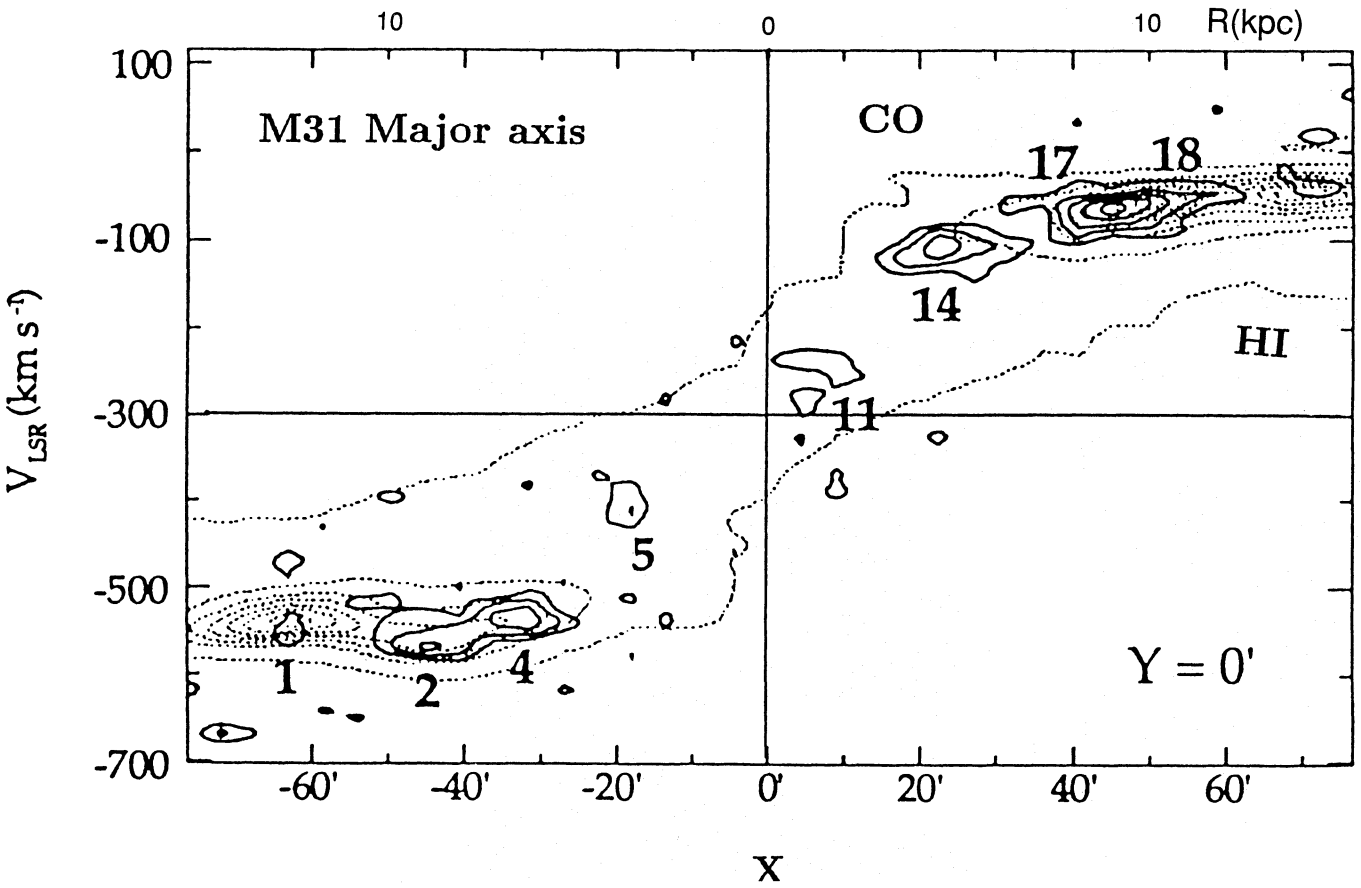

Fig. 4. CO + HI PV diagram along the major axis of M 31 (reproduced from Dame et al. 1993)

because of the narrow primary-beam coverage ($\sim$ 1′). Young et al. (1988) have obtained a map for a wider area using the FCRAO 14-m telescope with an angular resolution 45″. We superpose their CO PV diagram on the same HI data in Fig. 5b.

In both figures (Fig. 5a and b) the CO emission is highly concentrated in the nuclear disk. Particularly, the high-resolution diagram in Fig. 5a shows a very compact nuclear disk of radius 10″ (750 pc), where the HI absorption is clearly visible against the radio continuum emission from the nucleus. A weak ring (arm)-like feature is visible in CO at a larger radius $R \sim 30''$, but its intensity cannot be compared to the nuclear dense disk. Thus, this galaxy exhibits an exceptionally high concentration of CO emission near to the galactic center.

Such anomalously high concentration of molecular gas might have been triggered by some rapid accretion mechanism, such as due to a merger, and should be deeply coupled with the AGN. On the other hand, the HI gas is widely distributed in the broad ring at $R = 1' - 2'$ (5 - 10 kpc) and in the outskirts with a flat rotation.

2.6. *Our Galaxy*

The Milky Way Galaxy has long been observed both in HI and CO, and many longitude-velocity ($l - V_{\rm lsr}$) diagrams have been published (Dame et al. 1987; Burton 1988; Combes 1992). Figure 6 shows a direct comparison of the HI and CO intensity distributions on the $l - V_{\rm lsr}$ diagram. Figure 7 shows a similar diagram of the CO vs HI comparison for the first quadrant of the galactic plane ($l < 90°$), where the radial velocity has been corrected for the galactic rotation of the Sun by $V = V_{\rm lsr} + 200 \sin l$ km s^{-1}, so that the Galaxy appears as if it was observed from outside as an edge-on galaxy.

The CO emitting region composes a prominent bright ridge on the PV diagram with the tangential (terminal) point at $l = 30°$, which corresponds to the so-called '4-kpc molecular ring'. The nuclear molecular disk is also evident in the CO emission as the high-velocity component at $l < 4°$. The HI emission region is distributed at larger radii, with the broad maximum starting at $l \sim 40°$, and composes the 10-kpc HI ring with an extended outskirts beyond the solar circle. In fact the HI emission is clearly visible at $V_{\rm lsr} < 0$, indicating that a substantial fraction of the HI gas is distributed beyond the solar circle, whereas the CO emission is hardly visible in this diagram at negative $V_{\rm lsr}$. On the other hand, the HI emission gets much weaker toward the center at $l < 30°$ where the CO makes the 4-kpc ring. From these diagrams it is clearly recognized that the CO gas is distributed in the inner edge of the HI ring and that the CO and HI avoid each other in the galactic scale.

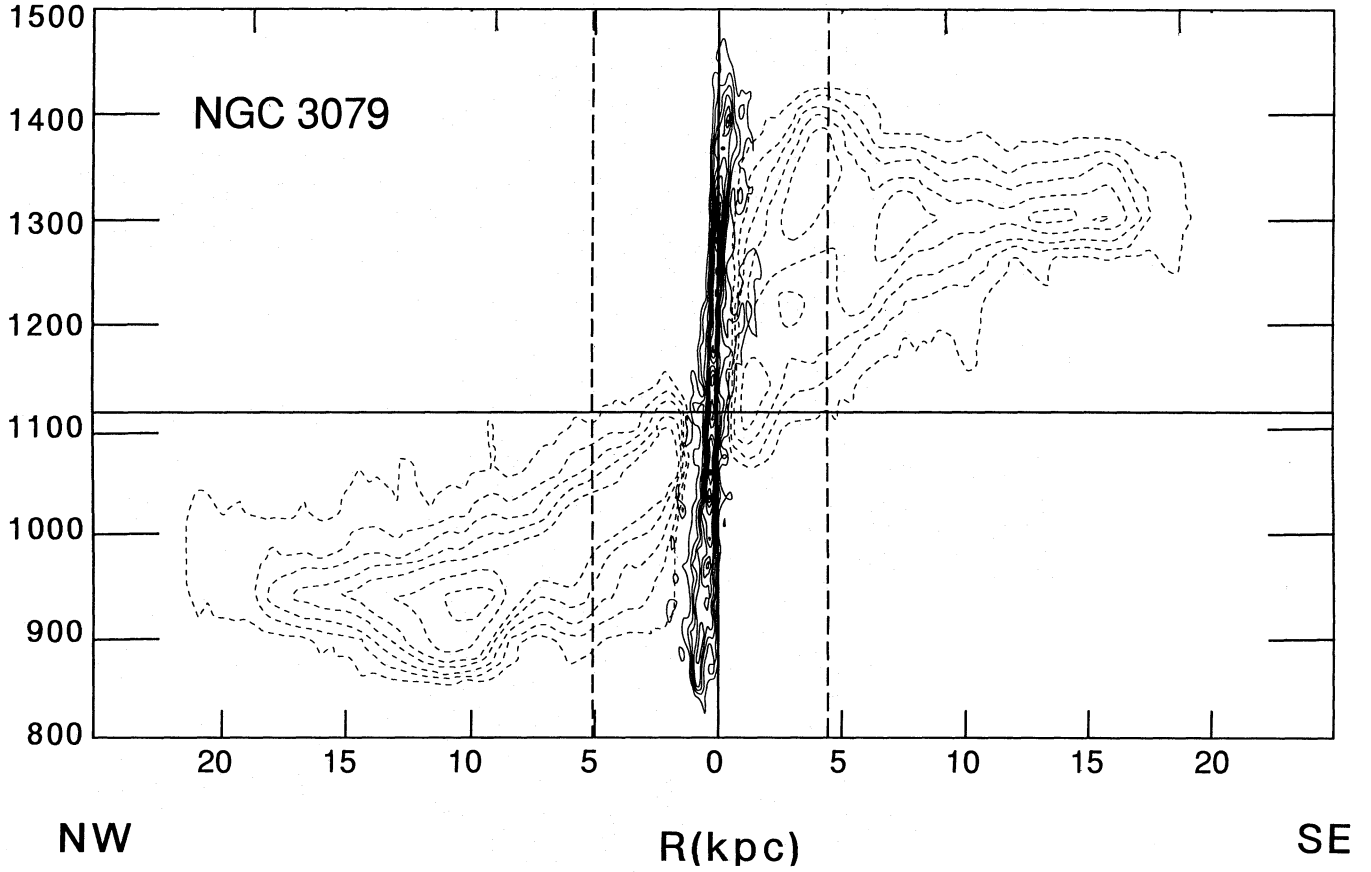

Fig. 5a. CO + HI PV diagram for NGC 3079, using CO data from the Nobeyama mm-wave Array

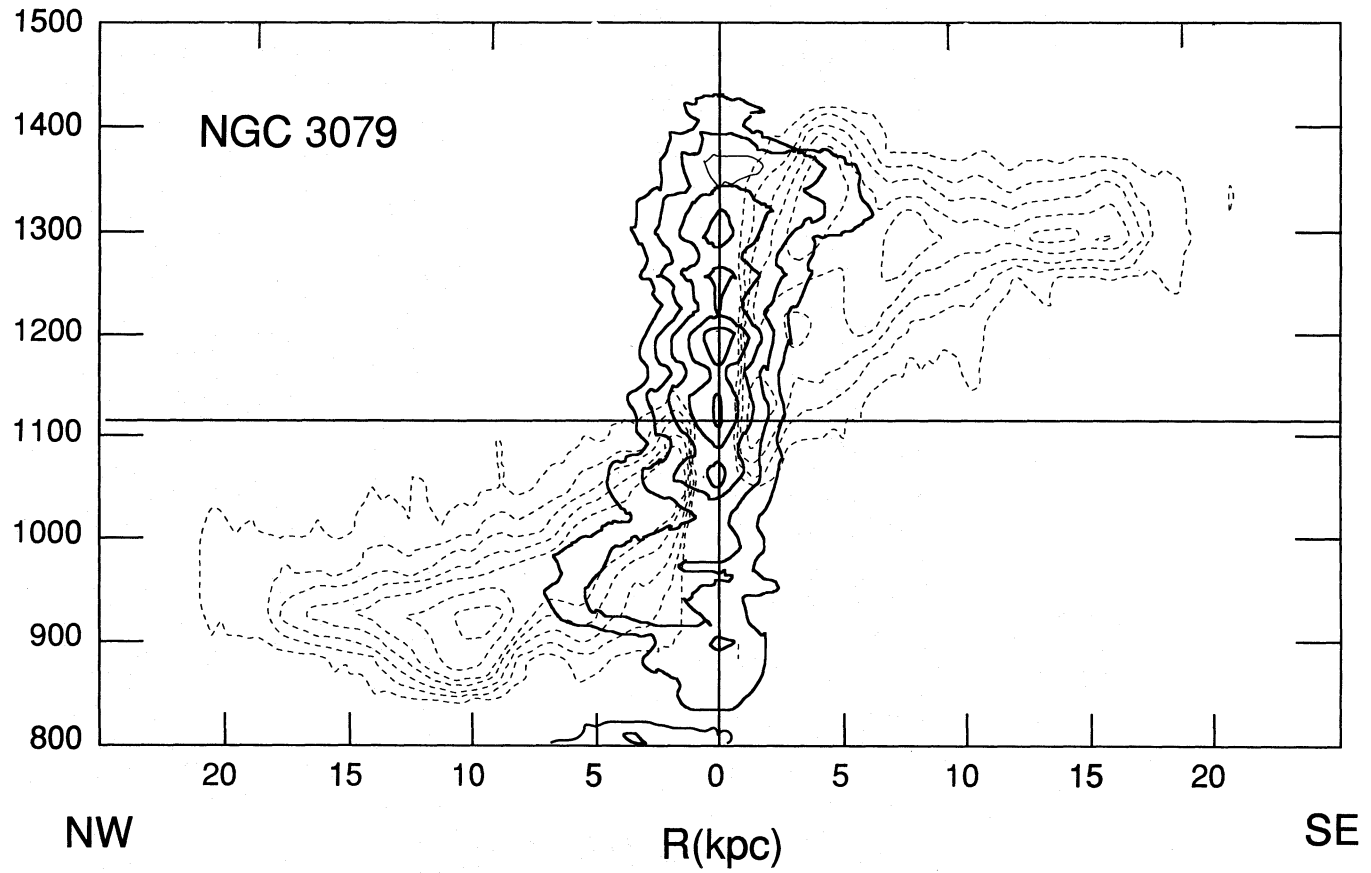

Fig. 5b. CO + HI PV diagram for NGC 3079, using the data FCRAO 14-m telescope (Young et al. 1988)

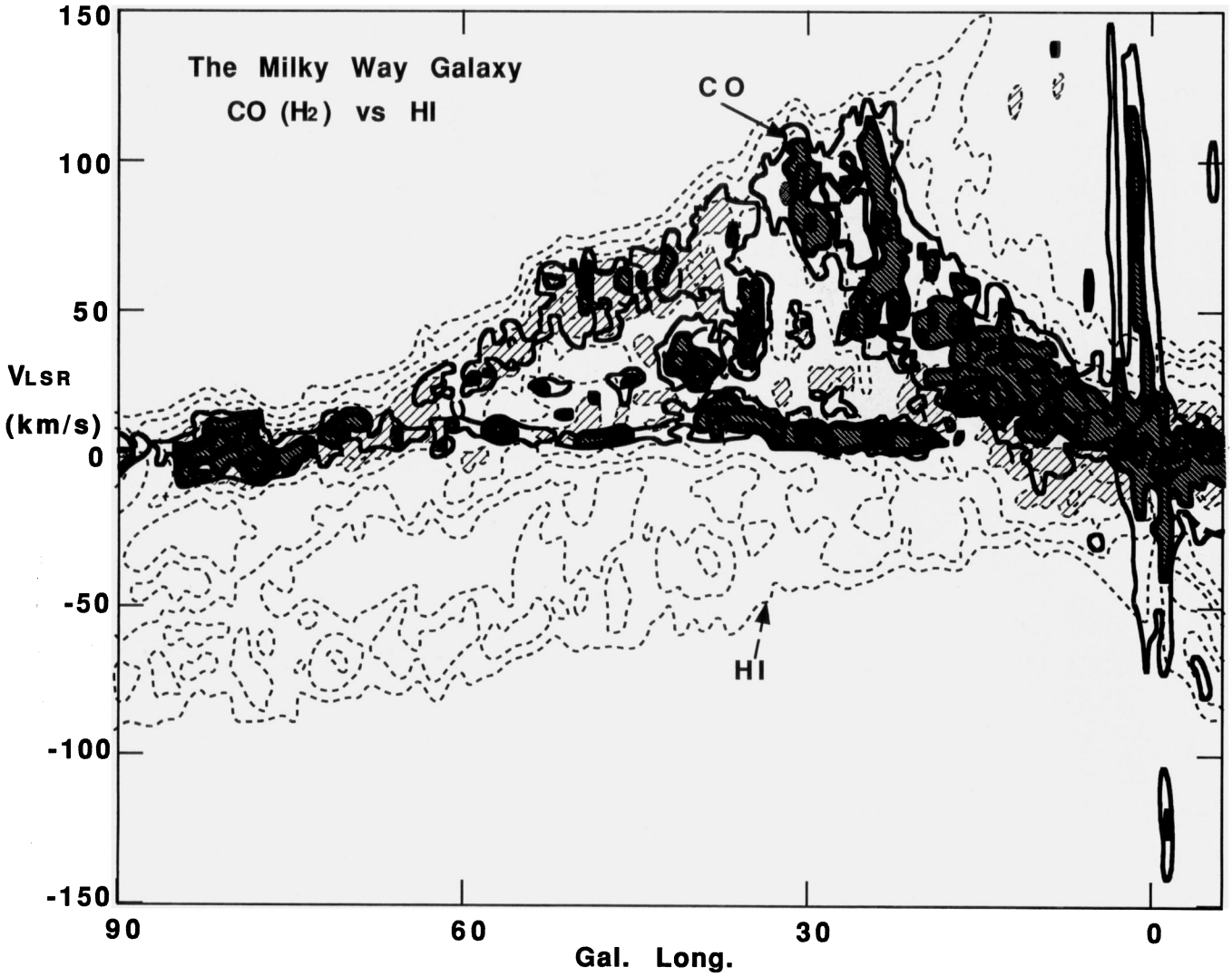

Fig. 6. CO + HI composite position-velocity ($l - V_{lsr}$) diagram for the Milky Way Galaxy

3. Radial variation of HI and H_2 densities

3.1. The CO-to-H_2 conversion factor

It is not a trivial matter if the CO-to-H_2 conversion factor is a universal constant, the conversion factors derived for spiral galaxies seem to lie within a range of a factor 2: $X \sim 2.3 - 4 \times 10^{20}$ H_2 cm^{-2} / K km s^{-1}(Bloemen et al. 1985; Maloney & Black 1988; Strong et al. 1993). Similar values to that in our Galaxy have been obtained also for virial clouds in spiral arms of M 31 (Vogel et al. 1987; Sofue et al. 1994), for M33 (Wilson & Scoville 1992), and for spiral arms in M51 (Nakai & Kuno 1994; Addler et al. 1992).

On the other hand, a larger value by an order of magnitude has been obtained for dark clouds in the inner region of M 31 (Allen & Lequeux 1993; Sofue & Yoshida 1993). This peculiar interstellar physics might be due to an infall of metal-deficient gas from merger companions into the central region of M 31, where no spiral arms can be traced (Sofue et al. 1994b; Sofue 1994b). Large conversion factors have been also derived for the Magellanic Clouds, which are both metal-deficient irregulars (Cohen et al. 1988; Rubio et al. 1993). In fact, it is known that the conversion factor is a sensitive function of the metallicity, and therefore, varies with the galacto-centric distance in each galaxy in the sense that it increases exponentially (as metallicity) with the radius (Arimoto et al. 1994).

Alternatively, the conversion factor could drastically increase with the radius, as Lequeux et al. (1993) have suggested: the outer Galaxy may be much richer in cold molecular gas without CO emission, because of the lack in sufficient UV photon from star-forming regions. In this case, the CO emission we are observing comes from warm molecular clouds around star forming regions, and therefore, the CO intensity is not directly related to the gas mass.

Although of the variety of values of the conversion factor thus far obtained, the values determined for normal disks in spiral galaxies from observations of CO-line intensity and virial masses appear to lie within a factor of two. In our following analysis, we adopt the conventional value: $C = 3.6 \times 10^{20}$ H_2/K

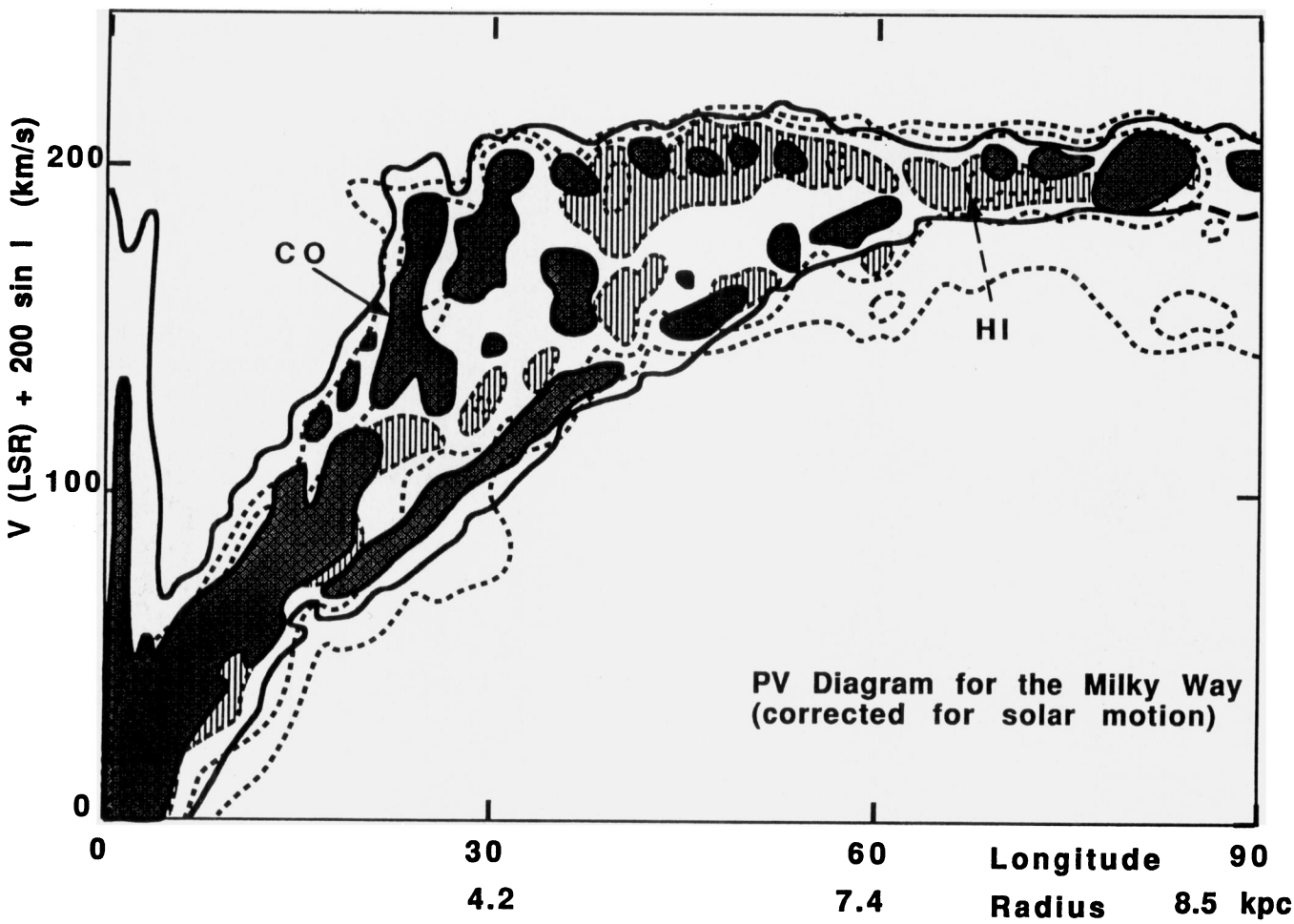

Fig. 7. A modified PV $[l - (V_{\rm lsr} + 200\sin l)]$ diagram for the Milky Way, where the Solar rotation has been subtracted

km s^{-1}(Sanders et al. 1984; Young & Scoville 1982). Different values of X within a range of a factor of 1.5 would not affect the conclusion in this paper.

3.2. Deconvolution method of PV diagrams

The gaseous distributions in the observed galaxies are characterized by a major molecular ring of a few kpc radius and an extended HI outskirts with spiral arms as well as the nuclear disk of molecular gas. Using the observed PV diagrams, we are able to derive radial density distributions both for the HI and molecular hydrogen by applying the de-convolving method proposed by Sofue & Nakai (1992).

By this method, the HI and H_2 densities in the galaxy disk at a radius R can be obtained by

$$n(\mathrm{HI}) = C_1 b_1^{-1} I_{\rm HI}/L, \tag{1}$$

$$n(\mathrm{H_2}) = C_2 b_2^{1} I_{\rm CO}/L, \tag{2}$$

where,

$$L = 2|R|\sqrt{V_{\rm rot}^2/V_{\rm min}^2 - 1}. \tag{3}$$

Here, C_1 and C_2 are the conversion factors from the intensities to column densities of H atoms and H_2 molecules, respectively and are given as $C_1 = 1.82 \times 10^{18}$ H cm^{-2}/(K km s^{-1}) and $C_2 = 3.6 \times 10^{20}$ H_2 cm^{-2}/(K km s^{-1}) (Sanders et al. 1984). The coefficients b_1 and b_2 are correction factors for the beam dilution in the z direction:

$$b_1 = 2z_{\rm HI}/\theta_1 D \tag{4}$$

and

$$b_2 = 2z_{\rm H_2}/\theta_2 D, \tag{5}$$

where $2z_{\rm HI} = 250$ pc (Dickey & Lockman 1990) is the scale thickness of the HI disk, $2z_{\rm H_2} = 150$ pc (Sanders et al. 1984) is the scale thickness of the molecular gas disk, θ_1 and θ_2 are the beam widths of the HI and CO observations, respectively, and D is the distance of the galaxy. The integrated CO intensity is given by

$$I_{\rm HI} = \int_{V_{\rm min}}^{V_{\rm max}} T_{\rm mb;\,HI}\, dV \ \ (\mathrm{K\ km\ s^{-1}}), \tag{6}$$

and

$$I_{\rm CO} = \int_{V_{\rm min}}^{V_{\rm max}} T_{\rm mb;\,CO}\, dV \ \ (\mathrm{K\ km\ s^{-1}}), \tag{7}$$

Table 1. Parameters for the deconvolution of position velocity digram

Galaxy Galaxy	V_{min} (km s^{-1})	V_{rot} (km s^{-1})	V_{max} (km s^{-1})	Distance (Mpc)
NGC 891 ...197	230	257	8.9	
NGC4565 ..240	260	280	10.2	
NGC5907 ..190	225	250	11.6	
NGC3079 ..200	230	260	15.0	

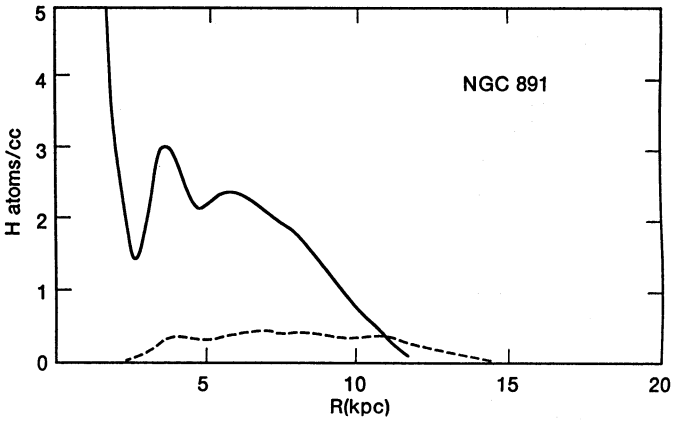

Fig. 8. The radial variation of the spatial density of H_2 and HI gases derived by de-convolution of observed HI and CO PV diagrams for NGC 891

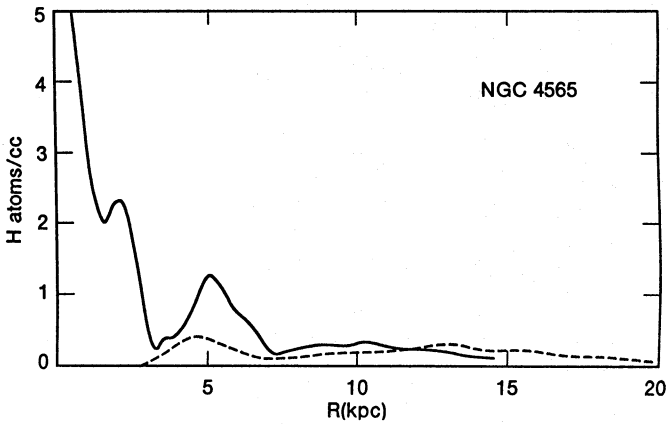

Fig. 9. The same, but for NGC 4565

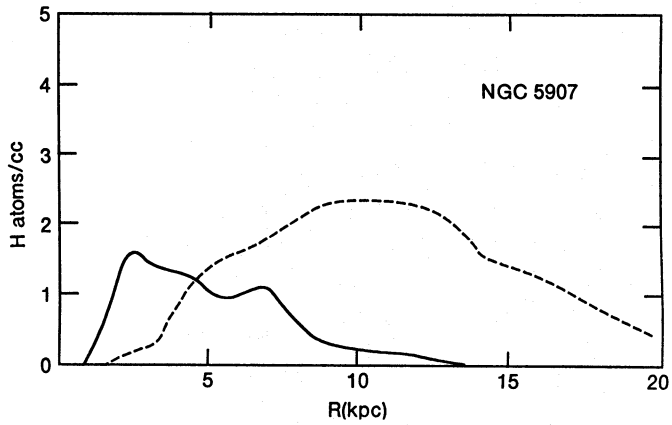

Fig. 10. The same, but for NGC 5907

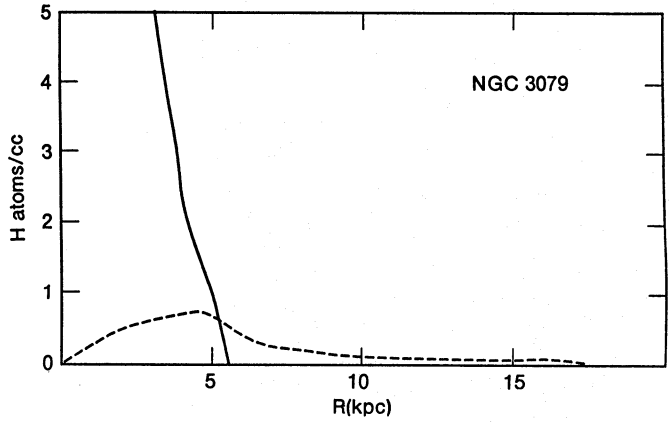

Fig. 11. The same, but for NGC 3079

where $T_{mb;\,HI,\,CO}$ are the main beam temperatures of the HI and CO emissions. The adopted values of V_{min}, V_{rot} and V_{max} in our calculations are listed in table 1, together with the adopted distances to the galaxies. The values of V_{max} are taken to be larger than the rotation velocity V_{rot} by 20~30 km s^{-1} in order to cover all the emission apparently beyond the terminal velocity due to the velocity dispersion in the interstellar gas. We have also used this method to obtain the HI density distribution for the same values of V_{min} and V_{max}.

We here assumed that the gas distribution is axisymmetric around the rotation axis, so that the obtained density is azimuthally averaged, and that the thickness of the gas disk is constant; 250 pc for the HI and 150 pc for the molecular gas disk. We also assumed that the rotation velocity is constant, which is a good approximation in most regions except in the nuclear disk and outskirts. In this method the error increases with decreasing radius toward the center, partly because of the deviation from flat rotation in the nuclear region and partly because of dividing by R which decreases toward the center. However, throughout the main part of the galactic disk this method was found to give quite reasonable results.

We have checked the validity of the thus obtained density distributions by applying some other different values of V_{min} from the above values, and ascertained that the results did not change so much. On the other hand, when we calculated the total HI and H_2 masses by integrating the obtained density over the entire disk, we obtained underestimated values compared to those found in the literature. The total H_2 mass is found to be smaller by a factor of 0.6 ~ 0.8 than the values in the literature calculated from observed total CO flux. The smaller amount of total mass from our calculation would be due to the present

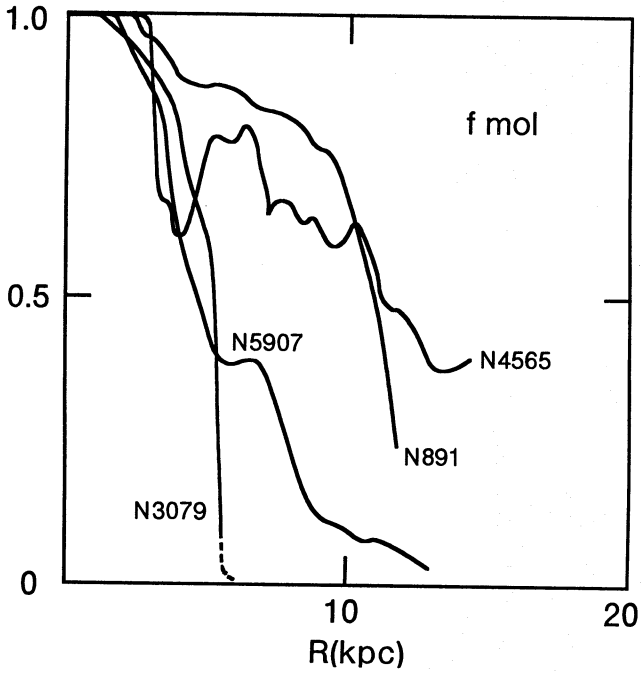

Fig. 12. The radial variations of molecular fraction, $f_{\rm mol}$, for the galaxies described in the text

approximation of azimuthal averaging, which ignores enhancements of density in the spiral arms or some local structures, and partly due to the fact that the galaxies contain extended molecular halos (Garcia-Burillo et al. 1992; Sofue & Nakai 1993). The HI masses from our calculation are smaller by a factor of $0.25 \sim 0.45$ than the values in the literature. This discrepancy is again thought to be due to the fact that the galaxies contain extended HI in the halo, while our results have been obtained only from the PV diagrams along the major-axis.

3.3. Radial distributions of the H_2 and HI densities

Figures 8 to 11 show the obtained distributions of HI and H_2 gas 1densities plotted against the radius for NGC 891, NGC 4565, NGC 5907 and NGC 3079. The unit of abscissa is H atoms cm^{-3}, where n(H) = $2n(H_2)$ for the molecular gas. Note that, except for NGC 3079, the beams used in the observations for the CO and HI lines are approximately the same (15″ and 20″, respectively). We make some comments about the density distribution of each galaxy below.

3.3.1. NGC 891

This galaxy contains a large amount of molecular gas, clearly showing the R = 4-kpc molecular ring and the nuclear disk. In larger scale the density of the H_2 gas decreases almost exponentially with the radius. On the other hand, the HI density is nearly constant throughout the major part of the disk, as widely known for normal galaxies. It is also remarkable that the HI gas exhibits significant depression in the central region at $R < 2$ kpc.

3.3.2. NGC 4565

In this galaxy, similarly to NGC 891, the 5-kpc molecular ring and the nuclear molecular disk are evident, as well as the approximately exponential decrease of the density with radius. On the other hand, the HI distribution is almost flat in the major disk extending to such large radius as 20 kpc or more. It is interesting to note that the 5-kpc molecular ring is also associated with a significant enhancement of HI gas.

3.3.3. NGC 5907

This galaxy shows a significant difference in the H_2 distribution from the other galaxies in the sense that the H_2 gas does not exist in the central 2 kpc region. As we have already seen in the PV diagram, this is due to the lack of the high-velocity component in the central region and the assumption of constant rotation velocity. We cannot ascertain the validity of this assumption for this galaxy, but it is worthwhile to note that there are some galaxies like M 31 which show a central depression of interstellar gas (Dame et al. 1993; Sofue & Yoshida 1993). We stress that NGC 5907 and M 31 may be two exceptions among Sb and Sc galaxies that usually have an exponentially decreasing density distribution with R.

3.3.4. NGC 3079

We have derived Fig. 11 using the low resolution CO data from the FCRAO 14-m telescope by Young et al. (1988) in order to see the large-scale density distribution. An anomalously high density concentration of the H_2 gas is found in the central $R < 5$ kpc region. On the other hand, no clear ring and outskirts are observed at larger radii than $\sim$ 5 kpc, and we cannot see any local structure like an arm in H_2 because of the large beam size of 45″(= 3.5) kpc in this diagram. It is known that the nuclear region shows a tight molecular ring at $R < 20''$) and the outer disk ($\sim 1'$) has a faint molecular arms (Sofue & Irwin 1992).

As mentioned above, this galaxy possesses an AGN, and therefore, it might be a merger. The anomalously high concentration of molecular gas would be a natural consequence, if there was a merger. However, it remains as a question, why only molecular gas has been accreted without sweeping the HI gas inward. Alternatively, as is proposed in this paper, the molecular concentration would be due to some high-conversion mechanism of HI into H_2 in the central region, such as due to anomalously high metallicity.

4. The molecular front

Although it is a matter of open discussion if the conversion factor from CO emission to H_2 mass is universal, we here simply adopt the conventional stand point of view. Then, the diagrams in Fig. 8 to 11, which are actually diagrams showing the emissivity, can be taken as showing the gas distributions. Using these distributions, we have derived radial variation of molecular-gas

fraction against the total gas density. We define the molecular fraction by

$$f_{\rm mol} = \frac{\rho_{\rm H_2}}{\rho_{\rm HI} + \rho_{\rm H_2}} = \frac{2n_{\rm H_2}}{2n_{\rm H_2} + n_{\rm H}}.$$

Figure 12 plots the obtained variation of the molecular fraction as a function of the radius R for NGC 891, NGC 3079, NGC4565, and NGC 5907.

All the plots in Fig. 12 show that the H_2 gas is dominant in the inner region of the galactic disk, while HI is dominant in the outer region. The molecular fraction is almost unity in the central few kpc region, and it decreases drastically at a critical radius. It is remarkable that the sudden decrease in the molecular fraction occurs in positional coincidence with the molecular ring of a few kpc radius: The sudden decrease occurs at $R \sim 3-4$ kpc in NGC 891, NGC 4565 and NGC 5907, and at $R \simeq 4-5$ kpc in our Galaxy. The molecular fraction, then, decreases to almost zero at $R \sim 10$ kpc. The galaxy disk is, therefore, separated into two parts at this critical radius; the inner molecular region, where the interstellar gas is almost totally H_2, and the outer HI region, where the gas is almost totally HI.

We stress that the transition from HI to H_2, and vice versa, is taking place within the very narrow range of radius, at the inner edge of which the molecular ring is located. We call such a clear border between the two regions of the disk the 'molecular front'. This front may be the manifestation of a galactic-scale phase transition between HI and H_2, and can be deeply coupled with the evolution of the interstellar gas.

It is remarkable that *all* the galaxies studied here have shown similar variations of the molecular fraction as a function of the galacto-centric distance. In the AGN galaxy NGC 3079, this transition occurs in a very inner region, where the the molecular gas is anomalously highly concentrated, while the outer disk is almost totally HI. In spite of the peculiar concentration of molecular gas near the AGN, which might be due to merger, the general behavior of the molecular fraction is almost the same as for the normal galaxies. Thus, the molecular front phenomenon appears to be a common feature in any types of galaxies.

In order to explain this molecular front phenomenon, we may consider some models. Here, we highlight the simple HI to H_2 transition theory in the ISM as proposed by Elmegreen (1993), which takes into account the gas density (pressure), metal abundance, and the UV photon intensity (star-formation activity).

Elmegreen (1993) has recently discussed the molecular fraction in a uniform ISM which is composed of spherical clouds of various masses. Suppose that a single spherical cloud is composed of two zones (an inner H_2 core and an outer HI envelope) and is embedded in a uniform ISM in a pressure balance. Then, given the mass of the cloud, the transition from HI to H_2, and vise versa, simply depends on the gas pressure (P), the strength of the dissociative-radiation (UV photon) field (U), and the heavy element abundance (Z) related to the amount of interstellar dust which shields the UV photon. The molecular fraction of the cloud increases, if the pressure and/or the heavy-element abundance increase, and if the dissociative UV intensity decreases. The transition is particularly sensitive to the heavy-element abundance and gas pressure.

The fraction is also an increasing function of increasing mass of the cloud. Once a distribution function of cloud masses is given, we can integrate molecular fractions for individual clouds to yield an averaged value of the molecular fraction ($f_{\rm mol}$) in a certain area of the gas disk of a galaxy. It is known that the temperature and velocity dispersion of the molecular as well as HI gas clouds do not vary so steeply with the radius in a galaxy disk (e.g., Kulkarni & Heiles 1988). We may, therefore, assume that the pressure is proportional to the total (HI + H_2) gas density, which can be approximately expressed by an exponential disk of scale radius of a few kpc. The radiation field can be assumed to be proportional to the star-formation rate which is a simple power-law function of the gas density (e.g., Kennicutt 1989). The metal abundance is known to be an exponential decreasing function of the radius (Díaz 1989; Belly & Roy 1992). In our recent paper (Sofue et al. 1994), we have shown that the molecular front phenomenon can be well reproduced by a simple simulation based on such simple assumptions as above in the scope of the phase-transition theory. In a forthcoming paper (Honma et al. 1994) we perform detailed theoretical simulations of the molecular-front phenomenon in galaxies based on more realistic approximations and models of galaxy disks.

References

Addler, D.S., Lo, K.Y., Wright, M.C.H. et al., 1992, ApJ 392, 497
Allen, R.J., Lequeux, J. 1993, ApJ 410, L15
Arimoto, N., Sofue, Y., Tsujimoto, T. 1994, submitted to ApJ
Belly, J., Roy. J.-R. 1992, ApJ 78, 61
Bloemen, J.B.G.M., Strong, A.W., Cohen, R.S. et al., 1985, A&A 154, 25
Bosma, A. 1981, AJ 86, 1791
Brinks, E., Bajaja E. 1986 A&A 169, 14
Burton, W.B. 1988, in Galactic and Extragalactic Radio Astronomy, ed. G. L. Verschuur, K. I. Kellermann (Springer Verlag, Berlin), pp. 295-358
Combes, F. 1992 ARA&A 29, 195
Dame, T.M., Koper, E., Israel., F.P. et al., 1993 ApJ 418, 730
Dame., T.M., Ungerechts, H., Cohen, R.S. et al., 1987, ApJ 322, 706
Díaz, A.I. 1989, in Evolutionary Phenomena in Galaxies, eds. J.E. Beckman, B.E.J. Pagel (Cambridge Univ. Press, Cambridge), p. 377
Dickey, J.M., Lockman, F.J. 1990, ARA&A 28, 215
Garcia-Burillo, S., Guélin, M., Cerhicharo, J. et al., 1992 A&A 266, 210
Elmegreen, B.G. 1993, ApJ 411, 170
Honma, M., Sofue, Y., Arimoto, N. 1994, in preparation
Irwin, J.A., Seaquist, E.R. 1991, ApJ 371, 111
Irwin, J.A., Sofue, Y. 1992, ApJL 396, L75
Kulkarni, S.R., Heiles, C. 1988 in Galactic and Extragalactic Radio Astronomy, ed. G.L. Verschuur, K.I. Kellermann (Springer Verlag, New York), Chap. 3
Kennicutt, Jr.R.C. 1989 ApJ 344, 685
Lequeux, J., Allen, J.R., Guillotearu, S. 1993, A&A 280, L23
Roberts M.S. 1978 AJ 83, 1026
Rupen, M.P., 1991, AJ 102, 48

Sancisi, R. 1976, A&A 53, 159
Sanders, R.H. 1977, ApJ 217, 916
Sanders, D.B., Solomon, P.M., Scoville, N.Z. 1984 ApJ 276, 182
Schöniger, F., Sofue, Y. 1993, A&A in press
Scoville, N.Z., Thakker, D., Carlstrom, J.E., Sargent, A.E., 1993, ApJ 404, L63
Sofue, Y. 1991, PASJ 43, 671
Sofue, Y. 1992, PASJ 44, L231
Sofue, Y. 1994a, PASJ 46, 173
Sofue, Y. 1994b, ApJ 423, 207
Sofue, Y., Honma, M., Arimoto, N. 1994a submitted to AAL
Sofue, Y., Irwin, J. 1992, PASJ 44, 353
Sofue, Y., Kato, T. 1981 PASJ 33, 449
Sofue, Y., Nakai, N. 1993, PASJ 45, 139
Sofue, Y., Nakai, N. 1994, PASJ 46, 147
Sofue, Y., Takabayashi, M. and Murata, Y. 1994, ASP Conf. Series No. 59, Astronomy with Millimeter and Submillimeter Interferometry, IAU Coll. No. 140., ed. M. Ishiguro and W.J. Welch, pp. 366-367
Sofue, Y., Yoshida, S. 1993 ApJL 417, L63-L65
Sofue, Y., Yoshida, Y., Aoki, T. et al., 1994b PASJ 46, 1
Strong, A.W. ,Bloemen, J.B.G.M., Dame, T.M. et al., 1988, A&A 207, 1
Vogel, S.N., Boulanger, F., Ball, R. 1987, ApJ 321, L145
Wilson, C.D., Scoville, N. 1992, ApJ 512
Young, J.S., Claussen, M.J., and Scoville, N.Z. 1988 ApJ 324, 115
Young, J.S., and Scoville, N.Z. 1982, ApJ 258, 467
Young, J.S., Scoville, N Z 1992, ARA&A 29, 581

This article was processed by the author using Springer-Verlag TEX A&A macro package 1992.